Cellular Physiology and Biochemistry

Cell Physiol Biochem 2018;45:319-331
DOI: 10.1159/000486813
Published online: January 24, 2018
Accepted: December 10, 2017

Original Paper

Skeletal Extracellular Matrix Supports Cardiac Differentiation of Embryonic Stem Cells: a Potential Scaffold for Engineered Cardiac Tissue

Xian Hong[a,b,c] Yin Yuan[a] Xiaoxi Sun[b,c] Meiling Zhou[b,c] Guangyu Guo[b,c] Quan Zhang[b,c] Jürgen Hescheler[d] Jiaoya Xi[b,c]

[a]Department of Anaesthesiology and Critical Care, Union Hospital, Tongji Medical College, Huazhong University of Science and Technology, Wuhan, [b]Department of Physiology and Chinese-German Stem Cell Center, School of Basic Medicine, Tongji Medical College, Huazhong University of Science and Technology, [c]The institute of Brain Research, Huazhong University of Science and Technology, Wuhan, China; [d]Institute for Neurophysiology, University of Cologne, Cologne, Germany

Key Words
Skeletal muscle • Extracellular matrix • Decellularization • Murine embryonic stem cells • Engineered cardiac tissue

Abstract
Background/Aims: Decellularized cardiac extracellular matrix (cECM) has been widely considered as an attractive scaffold for engineered cardiac tissue (ECT), however, its application is limited by immunogenicity and shortage of organ donation. Skeletal ECM (sECM) is readily available and shows similarities with cECM. Here we hypothesized that sECM might be an alternative scaffold for ECT strategies. ***Methods:*** Murine ventricular tissue and anterior tibial muscles were sectioned into 300 mm-thick, and then cECM and sECM were acquired by pretreatment/SDS/TritonX-100 three-step-method. Acellularity and morphological properties of ECM was assessed. SECM was recellularized with murine embryonic stem cells (mESCs) or mESC-derived cardiomyocytes (mESC-CMs), and was further studied by biocompatibility assessment, immunofluorescent staining, quantitative real-time PCR and electrophysiological experiment. ***Results:*** The relative residual contents of DNA, protein and RNA of sECM were comparable with cECM. The morphological properties and microstructure of sECM were similar to cECM. SECM supported mESCs to adhere, survive, proliferate and differentiate into functional cardiac microtissue with both electrical stimulated response and normal adrenergic response. Purified mESC-CMs also could adhere, survive, proliferate and form a sECM-based ECT with synchronized contraction within 6 days of recellularization. ***Conclusion:*** ECMs from murine skeletal muscle support survival and cardiac differentiation of mESCs, and are suitable to produce functional ECT patch. This study highlights the potential of patient specific of sECM to replace cECM for bioengineering ECT.

X. Hong and Y. Yuan contributed equally to this work.

Jiaoya Xi

Department of Physiology and Chinese-German Stem Cell Center, School of Basic Medicine, Tongji Medical College, Huazhong University of Science and Technology (China)
Tel. 0086-27-83692622, Fax 0086-27-83692608, E-Mail zhengyall@hotmail.com

Introduction

The engineered cardiac tissue (ECT) composed with suitable seeding cells and proper scaffold materials is an attractive method to replace diseased myocardium or reconstitution of cardiac malformations. Previous studies have demonstrated transplantation of ECT could prominently enhance the engraftment and survival of seeding cells in infarct myocardium and amplified their therapeutic efficacies after myocardial infarction (MI) [1, 2].

Up to date, a variety of natural and synthetic biomaterials have been evaluated as scaffolds in myocardial tissue engineering field. Concerning the capability to mimic native extracellular matrix (ECM) microenvironment, decellularized cardiac tissue has been considered as an attractive scaffold that preserves the architecture and biochemical composition of natural ECM [3, 4]. The main components of cardiac ECM (cECM) are collagens (type I, III and IV), fibronectin and laminin. They provide tissue-specific cues to support cell attachment, proliferation and differentiation [5, 6]. Generally, cECMs acquired by decellularization procedure are constituted of numerous of coiled and aligned fibril bundles and exhibit complex meshwork of pores [7]. Accumulated data have demonstrated that cECMs enhance the survival, proliferation, migration and cardiac differentiation of Sca-1^+ [4] or c-kit^+ [8] cardiac progenitor cells. It also accelerates differentiation of human induced pluripotent stem cells (iPS) derived cardiovascular progenitor cells towards the cardiomyocytes (CMs), smooth muscle cells or endothelial cells [9], and promote the elongation and alignment of neonatal CMs [4, 10]. Several studies have tested the possibility to employ non-cardiac ECMs as scaffolds to repair cardiovascular defects. Acellular small intestinal submucosa ECM (SIS-ECM) could be directly sutured in the damaged part of the heart. It provided a temporary biological scaffold for somatic cells from patients themselves, promoting cell proliferation and tissue repair [11]. In the animal model of MI, SIS-ECM [12] and urinary bladder ECM [13] had been shown to promote differentiation of mesenchymal stem cells (MSCs) towards CMs and improve heart function. However, the utilization of both cECM and above mentioned non-cardiac ECMs is limited for the shortage of patient-specific autogenous tissue and the risk of immune response from xenogenous ECM. Thus, new biocompatible patient-specific muscle-derived scaffold with low immunogenicity for ECT construction should be found. Skeletal muscle presents similar structure with cardiac muscle [14], belonging to striated muscle tissue. Skeletal ECM (sECM) also shows similarities with cECM, preserving the native architecture and mechanical properties suitable for implantation. SECM is subdivided into endomysium, perimysium, and epimysium [15] with a net like pattern. Similar to cECM, sECM is also mainly constituted of collagens (type I, III and IV), fibronectin, laminin and variety of growth factors [16, 17]. Collagen is thought to be the primary load bearing protein. The perimysium is composed by Type I and type III collagens. The basement membrane is comprised of laminin, type IV collagen and fibronectin [16]. Researches have demonstrated that sECM molecules play vital roles in cell migration, stabilization of cell with surrounding connective tissue, proliferation of myogenic progenitor cells, and subsequent stages of differentiation required to form new myofibers [18, 19]. Currently, sECMs are mainly used to construct engineered skeletal muscle tissue [20] for therapeutic strategies of abdominal wall defect [21] and hindlimb ischemia [22]. Compared with cECM, SIS-ECM and urinary bladder ECM, acellular sECM are more readily obtained from patients themselves avoiding immune rejection.

In the present study, we hypothesized that sECM is an alternative scaffold to replace cECM for ECT strategies. Herein, ECMs were obtained by parallel decellularization of adult mouse anterior tibial muscles (ATM) and ventricles thereby ensuring reliable comparison. Our results demonstrated that ECMs from skeletal muscle support survival and cardiac differentiation of murine embryonic stem cells (mESCs), and produce functional ECT patch with spontaneous beating and stimulated response, suggesting their potentials for cardiac tissue engineering applications.

Materials and Methods

Ethics Statement

All animal work in the present study was conducted according to the relevant national and international guidelines and was approved by Hubei Science and Technology Agency (2005-50).

Preparation of decellularized ECM slices of ventricle tissues (VTs) and ATMs

10-week-old KM male mice were anesthetized with intraperitoneal injection of sodium pentobarbital (50 mg/kg). The VTs were acquired, embedded in 4% low-melting agarose, and sectioned into 300-μm-thick slices by using a vibratome (Leica) as described previously [23]. The ATMs were cut into 5 mm×4mm×6mm blocks before embedded to control the dimension of tissue for slicing, and then sectioned into 300-μm-thick slices along 45°angle to the long axis. All the slices were kept in 4°C Ca^{2+}-free Tyrode's solution with continuously supply of pure oxygen before decellularization.

The decellularization procedure consisted of three steps: pretreatment, SDS treatment and Triton X-100 treatment. Firstly, the slices were pretreated with 0.05% (w/v) trypsin supplemented with 0.02% (w/v) EDTA for 30 min, 1.1% NaCl in double distilled water (DDW) for 30 min, and 0.7% NaCl in DDW for 30 min, respectively. Then the slices were incubated in 0.1% sodium dodecyl sulfate (SDS) in DDW for different hours (6, 7 and 8 h for ATM slices; 7.5, 9.5 and 11.5 h for VT slices). Finally, the slices were treated with 1% (w/v) Triton X-100 in PBS for 30 min. The diameter of cECM was about 4∼5 mm. The length and width of sECM was about 4 mm and 3 mm, respectively.

To compare the cell removal efficiency of each decellularization step, slices of VTs and ATMs were divided into three groups. The ECMs acquired by all the three steps of decellularization were named PreST group. To the PreS group, all the slices were undergoing pretreatment and SDS treatment. The slices of ST group were decellularized by SDS and Triton X-100 treatment without pretreatment. All the above mentioned steps were performed on the shaker at 37°C. Three times washout with PBS for 10 min were done between each step. The ECM slices were washed with ice-cold PBS contained 1% penicillin/streptomycin at least for 24 h to remove the residual detergents, and were ready for the following experiments.

Quantitative detection of DNA, protein and RNA

For total genomic DNA detection, specimens were incubated in TNE buffer, 10 % (w/v) SDS and proteinase K (10mg/ml) by volume to digest tissues. Then total DNA was extracted by phenol/chloroform method. The concentration of DNA was detected by spectrophotometry (NanoDrop 2000, Thermo Fisher Scientific) at 260 nm. The protein of each sample was lysed in RIPA (Boster) and quantified with the BCA Protein Assay Kit (Boster) according to the manufacturer's instructions. Total RNA of each sample was extracted by trizol (Invitrogen) extraction method and detected with a spectrophotometer at 260 nm. The relative residual DNA, protein and RNA contents of each sample were calculated by dividing the sample tissue weight before decellularization. Total DNA, protein and RNA of native slices served as positive controls.

Confirmation of acellularity

Samples were embedded in Tissue-Tek OCT compound (Sakura) and cross-sectioned into 8 μm serial sections for staining with haematoxylin-eosin (HE, Goodbio) and oil red O (Sigma) according to the manufacturer's instructions. For Masson staining, the samples were embedded in paraffin, sliced into 5 μm serial sections (Leica) and stained according to the manufacturer's instructions. All sections were observed by inverted microscopy (OLYMPUS).

Transmission electron microscopy (TEM) and scanning electron microscopy (SEM)

TEM and SEM were utilized to observe components and topography of decellularized ECM. For TEM, the examples were fixed with 4% paraformaldehyde, then postfixed in 1% phosphate-buffered OsO_4 and embedded in epoxy resin. 60-nm-thick sections were sliced and observed by a transmission electron microscope (FEI Technai G212). The diameter was measured manually using ImageJ software. For SEM, ECMs were fixed with 2.5% glutaraldehyde phosphate buffer, then dehydrated using graded ethanol and dried under vacuum. Then the dried ECMs were sprayed with platin/palladium. The surface structures were studied by a scanning electron microscopy (INCAx-act).

Cultivation of mESCs and mESC-derived CMs (mESC-CMs)

The transgenic mESCs (clone αPIG44) was maintained as previously described [24]. Briefly, undifferentiated mESCs were cultured in IMDM containing 15% FCS, 1% nonessential amino acids, 2mM L-glutamine, 0.1 mM β-mercaptoethanol, 100 U/mL penicillin, 100 μg/mL streptomycin and 1000 U/mL leukemia inhibitory factor (LIF, Chemicon). The purified GFP-positive mESC-CMs were harvested by mass culture protocol as previously described [23]. Puromycin (10 μg/mL, InvivoGen) was added at day 9 and day 12 during the whole differentiation period [25]. Between day 14 and 16 of differentiation, the mESC-CMs were collected and digested into single cells by trypsin and used for following experiments.

Recellularization of ECM with mESCs or mESC-CMs

We designed a modified hanging drop method [23] to enhance the direct contact between seeded cells and ECM. Briefly, a single decellularized ECM was carefully spread on a sterilized lid of 90 mm petri dish. 30 μL of cell suspension which contained 2, 500, 5, 000 or 10, 000 mESCs were carefully suspended over half-dried ECM without bubble generation. Then the lid was carefully turned over to form a hanging drop containing a single ECM with surrounding cells. 12 mL of PBS were added into the dish to avoid the hanging drop drying out. After 2 days, the recellularized ECM was carefully transferred into a 48-well plate, and cultured with IMDM containing 20% FCS, 1% nonessential amino acids, 2mM L-glutamine, 0.1 mM β-mercaptoethanol, 100 U/mL penicillin and 100 μg/mL streptomycin for another 2 weeks.

400, 000 mESC-CMs were seeded on ECM by above mentioned hanging drop method and cultured for 6 days. The medium was changed every day. Images were acquired every 2 days of the whole culture period.

Biocompatibility assessment of sECMs

MESCs and mESC-CMs were seeded in 24 well plates and cultured with the above stated medium, respectively. Once the cells grew to 70% confluence, the medium was replaced by 200 μL fresh medium and the cells were exposed to acellular ECMs for 12 h. Native slices of ATMs and VTs served as positive controls, the wells with no native tissue slices or ECMs served as blank controls for basal nitric oxide (NO) secretion. According to the manufacturer's instructions, NO_2^- concentration were measured and determined against a standard calibration curve using the Griess reagent system G2930 (Promega). Live/Dead Viability/Cytotoxicity Kit (Invitrogen) was used to assess the viability of mESCs grown on the substrates during the whole recellularization period. 5, 000 mESCs were seeded at the beginning of recellularization. The specimens were incubated for approximately 10 min with 2 μM calcein AM and 4 μM EthD-1 in phosphate-buffered saline (PBS) at 37°C. Live and dead cells in each group were visualized under a fluorescence microscope (Zeiss CFM-500). AlamarBlue® cell viability reagent (Invitrogen) and LDH Cytotoxicity Assay Kit (Beyotime) were used to quantitatively measure cellular activity and cytotoxicity during recellularization according to the manufacturer's instructions. Before adding alamarBlue solution, cells which did not attached to ECMs were washed away with PBS.

Quantitative real-time PCR

Total RNA was extracted from recellularized ECMs using trizol according to the instructions of the manufacturer. The total RNA (3 μg) was reversely transcribed into cDNA using oligo (dT) primer and MMLV reverse transcriptase (Invitrogen). Real-time PCR was performed in the CFX Connect™ Real-Time PCR Detection System (Bio-Rad) using SYBR Premix Ex Taq (TOYOBO). CT values were automatically obtained. Relative expression of mRNA amount was calculated using the ΔΔCT method [26]. The primers used for real-time PCR are listed in Table 1.

Physiological function studies

Tyrode solution contained (in mM): NaCl 137, $NaHCO_3$ 15.5, NaH_2PO_4 0.7, $CaCl_2$ 1.8, KCl 4, $MgCl_2$ 1 and glucose 11.1 was prepared and gassed with purified oxygen. Before the experiments with MED64 Recording System, the MED probe (MED-P515A; Panasonic, Tokyo, Japan; each electrode: 50 × 50 μm, interpolar distance: 150 μm) was soaked in 70% ethanol for 15 min and dried

Table 1. Primers for real-time PCR analysis

Genes	Sense primers (5'-3')	Antisense primers (5'-3')	Product size (bp)
GAPDH	TGACCACAGTCCATGCCATC	GACGGACACATTGGGGGTAG	204
α-MHC	GATTTCTCCAACCCAGCTGCGCC	CGGATGTCAAAGGGCCGGGTC	201
MLC2v	TGTGGGTCACCTGAGGCTGTGGTTCAG	GAAGGCTGACTAGTGCCGGGAGATGC	189
ANP	GCCGCACTTAGCTCCCTCCCCGAG	GTACCGGAAGCTGTTGCAGCCTAG	241

up. The surface of the probes was treated overnight at 4°C with 0.1% polyethylenimine and 25 mM borate buffer, pH 8.4 [27]. The probe surface was dried and rinsed three times with deionized water. The specimen was gently mounted and forced to be contact with the surface of the probe by a custom made slice anchor. The whole system temperature was kept at 37°C and perfused with Tyrode solution. We set the stimulate intensity with 10 μA electric current and 2.3 mV voltage. The high pass filter frequency was 10 Hz and the low pass filter frequency was 1000 Hz. The gain of the system was 50 and sampling rate was 20 kHz. The specimen was paced at 0.5 Hz, 1 Hz, 2 Hz, 3Hz, 4Hz and 6 Hz and the field potential (FP) amplitude was recorded by MED 64 recording system. The conduction velocity was measured by dividing the distance between two sites before and after treated with (-) misoproterenol (Iso, 1μM) at 0.1 Hz.

Immunofluorescent staining

Cryosections (8 μm) were permeabilized with 0.1 % Triton X-100 for 10 min. After being blocked with 5 % bovine serum albumin (BSA), specimens were incubated with monoclonal anti-α-actinin (1:1200, Sigma) or monoclonal anti-Cx43 (1:1500, Abcam). The fluorescent antibody was TRITC-conjugated goat anti-Mouse-IgG (1:80, SanYing) and TRITC-conjugated goat anti-rabbit IgG (1:100, SanYing), respectively. Nuclei were stained with DAPI (Sigma). Images were acquired by confocal microscopy (Olympus, FV1000).

Statistical analysis

Unless otherwise stated, the results were given as the mean ± SEM. The significance of differences between the means was evaluated by unpaired *t*-test. For multiple comparisons, data were analyzed by ANOVA followed by Tukey's post-hoc test. $P < 0.05$ were considered statistical significant. Statistical analyses were performed with SPSS 16.0.

Results

Preparation and characterization of ECM from ATM and VT

Both the fresh ATM and VT slices were light brown, and gradually became glossy translucent acellular matrixes with preserved inherent vasculature after decellularization with pretreatment, SDS treatment and Triton X-100 treatment (Fig. 1A). To ensure the optimal decellularization procedure, we next assessed the relative residual DNA contents in the native controls and ECMs obtained by different decellularization methods. Generally, the average relative DNA contents in all groups from skeletal tissues were significantly lower than those from cardiac tissues. The relative DNA contents were 556.65 ± 60.38 ng/mg (n = 5) in fresh skeletal tissue and 2019.67 ± 155.71 ng/mg (n = 8) in fresh cardiac tissue, respectively. For both skeletal and cardiac tissue, all the decellularized groups had extremely lower relative residual DNA contents than native controls (Table 2 and 3, VT n=8, ATM n=5, $p < 0.01$). Moreover, sECMs without pretreatment or TritonX-100 treatment had significantly higher residual DNA contents compared with ECMs undergoing three-step decellularization (n=5, $p < 0.01$ *vs*. ST group, $p < 0.05$ *vs*. PreS group), suggesting that both pretreatment and Triton X-100 are necessary for the effective decellularization of skeletal muscle. However, a prolonged SDS treatment seemed no effect on the residual DNA contents of ECMs from both ATM and VT (VT n=8, ATM n=5, $p > 0.05$). In the following experiments, 9.5 h and 7 h of SDS incubation were used for the generation of cECMs and sECM, respectively.

We also further assessed the relative residual protein and RNA contents in native control groups as well as ECMs from PreST group (Table 2 and 3). The ECMs from ATM had comparable relative residual protein contents to those from VT (1.29 ± 0.25 mg/g *vs.*1.58 ± 0.22 mg/g, n = 6) which were extremely lower than those native controls (n = 6, $p < 0.01$). Similarly, the relative residual RNA contents of ECMs from both ATM and VT were also comparable (16.03 ± 1.81 μg/g *vs.*12.59 ± 2.42 μg/g, n = 6), and extremely lower than native controls (n = 6, $p < 0.01$).

Histological assessment was also employed to examine the effect of each decellularization method on acellularity and structural preservation of the ECM scaffold. Consistent with the analysis of the relative residual DNA, protein and RNA contents, HE staining showed that for both ATM and VT, only PreST group resulted in complete decellularization of entire scaffolds,

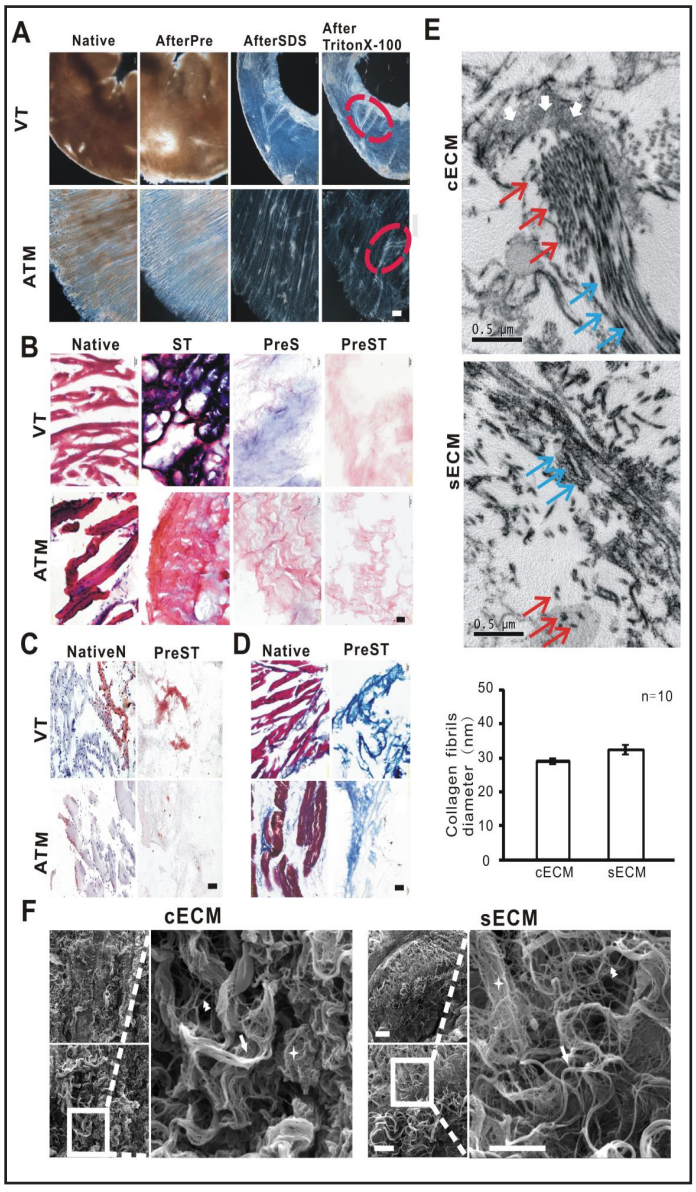

Fig. 1. Morphological characterization of ECMs from murine VT and ATM. (A) Representative light microcopy images of the slices from VT and ATM during decellularization procedure. Inherent vasculature structures (red circle) were preserved. (B) Representative images of HE staining of VT (upper row) and ATM (lower row) before and after different decellularization procedure. (C and D) Representative images of oil-red O staining (C) and Masson staining (D) of native controls (left) and ECM in PreST group (right). (E) Representative images of collagen fibers obtained by TEM (top) and mean diameter of fibril units (bottom). White arrows, elastic fibers; blue arrows, collagen fibrils; red arrows, cross section of collagen fibrils. Scale bar = 200 μm in (A), 20 μm in (B), (C), (D), and 0.5 μm in (E). (F) Representative SEM micrographs of cECM and sECM. Endomysium honeycomb-like structure was well preserved after decellularization (stars). Characteristic coils (arrows), struts (arror heads) were retained. Scale bar = 20 μm (left upper row), 10 μm (left lower row), and 5 μm (right). ST, decellularization with SDS treatment and Triton X-100 treatment; PreS, decellularization with pretreatment and SDS treatment; PreST, decellularization with pretreatment, SDS treatment and TritonX-100 treatment.

with no presence of nuclei or cellular remnants (Fig. 1B). Nucleic debris and cellular remnants were widely existed in ECMs of ST groups, and were also visible in ECMs of PreS groups. Furthermore, oil-red O staining revealed that the PreST groups resulted in a more efficient removal of adipose tissue from skeletal tissue than that from cardiac tissue (Fig. 1C). Masson staining further confirmed that both skeletal and cardiac ECMs of PreST groups preserved collagen fiber network (blue) with no muscular remnants

Table 2. Values of relative residual DNA, protein and RNA contents of each group of ventricular tissue. All data were presented as mean ± SEM. #, $p < 0.01$ vs. native group. *, $p < 0.05$ vs. PreST group. ST, decellularization with SDS treatment and Triton X-100 treatment; PreS, decellularization with pretreatment and SDS treatment; PreST, decellularization with pretreatment, SDS treatment and Triton X-100 treatment

Contents	n	Native	ST	PreS	PreST SDS 7.5h	PreST SDS 9.5h	PreST SDS 11.5h
DNA (ng/mg)	8	2019.67±155.71	436.31±13.37#*	76.94±16.54#	83.09±7.89#	80.34±8.29#	54.75±10.82#
Protein (mg/g)	6	194.66±10.02	/	/	/	1.58±0.22#	/
RNA (μg/g)	6	1094.08±107.83	/	/	/	12.59±2.42#	/

(red) (Fig. 1D). TEM also showed that sECM in PreST group preserved similar collagen fiber network structure and units to that of cECM (sECM: 32.13 ± 1.22 nm; cECM: 29.07 ± 0.82 nm). However, the elastin fiber was observed only in cECM (Fig. 1E upper). To examine the surface morphology and three-dimensional architecture of PreST ECM, both cECM and sECM were visualized under SEM (Fig. 1F). The endomysium honeycomb-like structure was well preserved in both groups. The alignment and organization of both perimysium fibers and smaller fibrillar weaves were also observed in both groups.

Above findings suggests that the collagen fibers with three-dimensional structure were well preserved in ECM of PreST group, while the cellular constituents were removed completely.

Table 3. Values of relative residual DNA, protein and RNA contents of each group of skeletal tissue. All data were presented as mean ± SEM. #, p < 0.01 vs. native group. *, p < 0.05 vs. PreST group. **, p < 0.01 vs. PreST group

Contents	n	Native	ST	PreS	PreST SDS 6h	PreST SDS 7h	PreST SDS 8h
DNA (ng/mg)	5	556.65±60.38	33.26±5.45#**	29.36±1.67#*	21.05±2.32#	16.95±1.56#	19.09±2.60#
Protein (mg/g)	6	110.04±9.67	/	/	/	1.29±0.25#	/
RNA (μg/g)	6	654.10±56.41	/	/	/	12.03±1.81#	/

Table 4. Nitrite Concentration (μM) by mESCs exposed to ECMs. N = 5 in each group. All data were presented as mean ± SEM. **, p < 0.01 vs. native group; *, p < 0.05 vs. native group; ##, p < 0.01 vs. cECM group.

	Sham	Native	PreST
cECM	1.20±0.16	19.16±1.35	0.94±0.10**
sECM	1.20±0.16	14.52±3.75	2.93±0.30*##

SECMs support adhesion, survival and proliferation of mESCs

We next used mESCs to further evaluate the biocompatibility of sECMs. Firstly, we cocultured ECMs with mESCs for 12 h and the NO secretion was measured. Native VT and ATM resulted in higher NO secretion. Although decellularization proved significantly decreased the NO level in both skeletal group and cardiac group, NO level was higher in sECM group (Table 4).

We further recellularized sECM and cECM by seeding 5, 000 mESCs with hanging drop method. Standard cardiac differentiation medium was used as described previously [23]. Live/Dead staining showed that many living mESCs aggregates (Green) attached to both sECM and cECM after two days culturing, gradually grew up and merged with adjacent aggregates during recellularization (Fig. 2A). However, a greater number of dead cells (Red) on cECM were observed at day 8 of recellularization, compared with those on sECM (Fig. 2A). We also seeded different number of mESCs on sECMs and observed recellularization via light microscopy. Light microscopy images showed that the sECM gradually became deeper in color and smaller in area during recellularization (Fig. 2B). HE staining further confirmed existence of numerous well-distributed cells in the interior of sECM (Fig. 2C), indicating the mESCs could adhere, survive and proliferate in sECM. We next quantitatively evaluated the biocompatibility of sECMs using LDH assay and alamarBlue assay at different days of recellularization after seeding different number of cells. Consistently, no significant difference in the LDH content was observed at different day of recellularization, except that the LDH content of the group seeding 10, 000 cells on day 16 was significantly higher than that on day 4 (Table 5). AlamarBlue assay (Table 6) showed that the value of fluorescence intensity increased gradually in each group, notably higher than that of day 4 and reached to the highest level on day 12, demonstrating the proliferation of cells in each group. At day 4, the fluorescence intensity in 10, 000 cells group was significantly higher than the other two groups. However, there were no differences at other time points between these groups, suggesting that the number of seeding cells has little effect on the later population of cells.

MESCs seeded on sECMs successfully differentiate into functional cardiac tissue

We also assessed the effect of sECMs on the cardiac differentiation during above mentioned recellularization. At day 16 of recellularization, GFP-positive cardiomyocyte clusters (Green) with spontaneous contraction were observed in 2, 500, 5, 000 and 10, 000

cells groups (Fig. 2B). We next analyzed the transcription levels of cardiac specific marks α-MHC, MLC2v and ANP at day 16 of recellularization. The mRNA expression levels of MLC2v in 5, 000 and 10, 000 cells groups were significantly higher than it in 2, 500 cells group ($p < 0.05$) (Fig. 2D), while no significant difference of α-MHC and ANP gene expression was found. We further studied the electrophysiological function of sECM-based cardiac tissue at day 16 of recellularization by recording the FP with MED64 recording system. The FPs were elicited by electrical stimulus at different frequencies (Fig. 3A). In addition, β-adrenergic agonist Iso (1 μM) could increase the amplitude of FP to 2.61 ± 0.35 times (0.49±0.18 mV *vs.* 1.20±0.35 mV; n = 3, $p < 0.05$) (Fig. 3B and C), and significantly increased the conduction velocity to 2.25 ± 0.28 times (0.29±0.17 m/s *vs.* 0.60±0.39m/s; n = 3, $p < 0.05$) compared with baseline (Fig. 3C), indicating the sECM-based cardiac tissue possessed normal adrenergic response. Collectively, these results indicate that mESCs seeded on sECMs successfully differentiate into functional cardiac tissue.

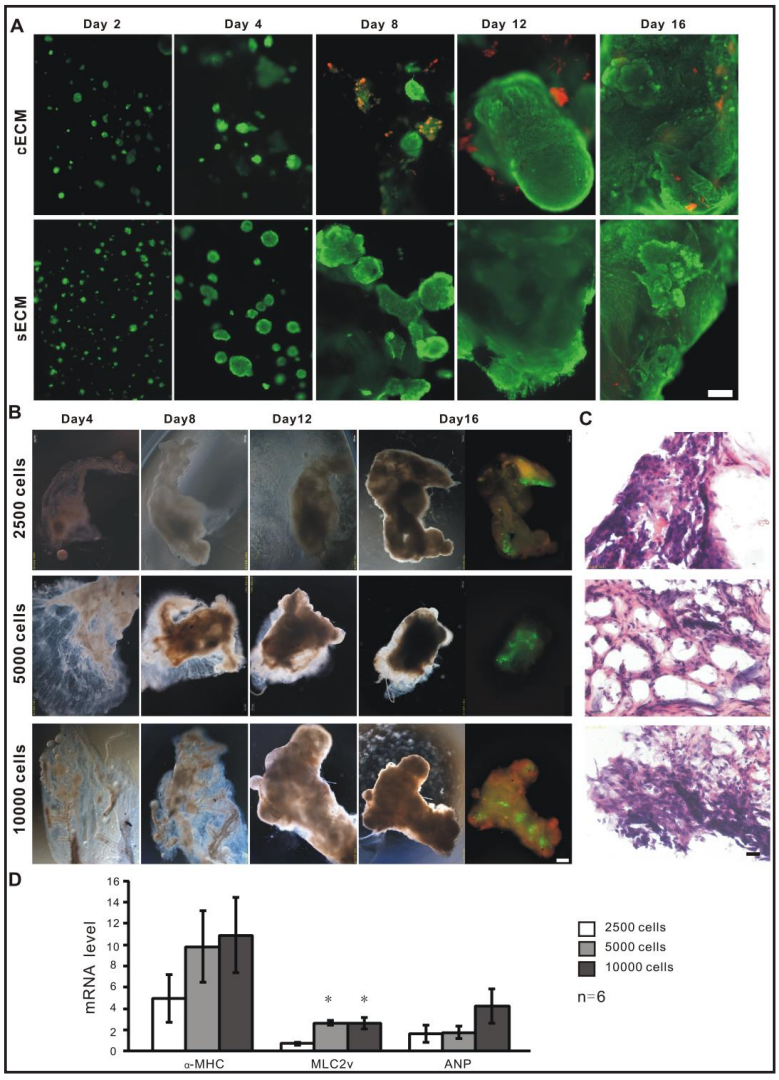

Fig. 2. SECMs support adhesion, proliferation and cardiac differentiation of mESCs. (A) Representative images of live/dead staining during recellularization of cECM (upper) and sECM (lower) with mESCs. 5,000 of mESCs was stained with calcein-AM (green)/ethidium homodimer (red) and seeded on ECMs. (B) Representative sequential light micrographs of sECM recellularized with different number of mESCs and fluorescence micrographs on day 16. GFP-positive cells (Green) were CMs differentiated from mESCs cultured on sECM. (C) Representative images of HE staining on day 16 of recellularization. Scale bar = 400 μm in (A), (B) and 40 μm in (C). (D) The expression of cardiac-specific markers on day 16 of differentiation. All data were presented as mean ± SEM; n = 6; *, p<0.05 vs. 2,500 cells group. α-MHC, α myosin heavy chain; MLC2v, myosin light chain 2v; ANP, atrial natriuretic peptide.

SECMs support adhesion, survival and proliferation of purified mESC-CMs

To further assess whether sECM was appropriate for cultivating CMs, we firstly cocultured ECMs with mESC-CMs for 12 h and the NO secretion was measured. The NO level

in both skeletal group and cardiac group decreased significantly when compared with that in native groups (Table 7). Then we recellularized sECM with purified mESC-CMs by the same hanging drop methods. The GFP-positive mESC-CMs adhered to sECM (Fig. 4A), and showed spontaneous contraction from day 4 to day 6 of recellularization. The contraction frequency was 136 ± 7 beats/min on day 4 and 110 ± 8 beats/min on day 6 of recellularization. There were no significant difference between the LDH content at day 4 and day 6 of recellularization (n = 6, $p > 0.05$) (Fig. 4B). The fluorescence value detected by alamarBlue assay at day 6 was notably higher than that of day 4 (n = 4, $p < 0.05$) (Fig. 4C). HE staining showed the presence of cell clusters at both out surface and inner core area of sECM, indicating the migration of mESC-CMs into the core area of sECM scaffold (Fig. 4D). Immunostaining confirmed that the GFP-positive cell clusters expressed the cardiac specific mark α-actinin and Cx43 (Fig. 4E).

Table 5. LDH release (absorbance value) at different day of recellularization. Detection wavelength was 562 nm. N = 5 in each tested group. All data were presented as mean ± SEM. *, p < 0.05 vs. day 4 of the same group

	Day 4	Day 8	Day 12	Day 16
2500 cells	0.11±0.05	0.40±0.15	0.38±0.16	0.37±0.17
5000 cells	0.19±0.05	0.58±0.26	0.43±0.13	0.43±0.13
10000 cells	0.10±0.03	0.13±0.07	0.40±0.20	0.44±0.13*

Table 6. AlamarBlue assay (fluorescence value) at different day of recellularization. Excitation wavelength was 560/40 nm, emission wavelength was 645/40 nm. N = 5 in each tested group. All data were presented as mean ± SEM. *, p < 0.05 vs. day 4 of the same group. **, p < 0.01 vs. day 4 of the same group. #, p < 0.05 vs. day 4 of 2,500 cells group. ##, p < 0.01 vs. day 4 of 2,500 cells group

	Day 4	Day 8	Day 12	Day 16
2500 cells	658.6±80.6	1659.8±141.0**	2193.6±193.3**	2045.4±143.3**
5000 cells	977.0±93.1#	1785.4±113.1**	2310.9±201.5**	2132.2±155.4**
10000 cells	1035.5±62.3##	1883.4±269.1*	2332.0±252.8**	2045.8±205.2**

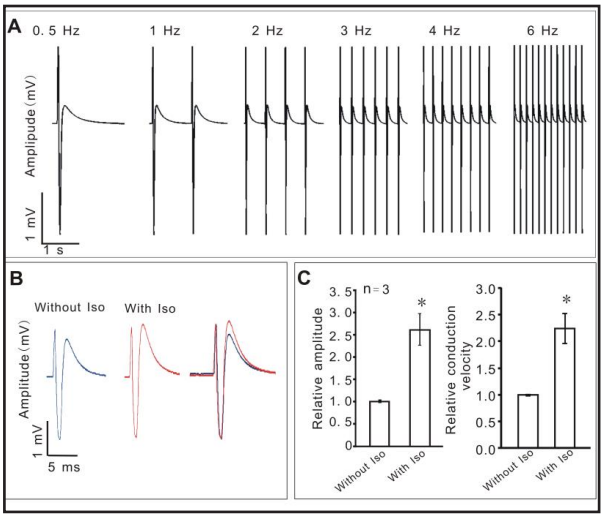

Fig. 3. Field potential (FP) of sECM-based cardiac tissue recorded on day 16. (A) Representative graphs of FP at different stimulus frequencies. (B) FP of sECM-based cardiac tissue before and after treated with Iso under 0.1 Hz stimulation. (C) Conduction velocity of FP was significantly increased after treated with 1μM Iso. All data were presented as mean ± SEM. *, p<0.05 vs. conduction velocity without Iso. Iso, (-) isoproterenol.

Discussion

The main findings of our study are: (1) sECM obtained by three-step decellularization shows similar structure pattern to cECM; (2) sECM supports mESCs to adhere, survive, proliferate and differentiate into functional CMs; (3) purified mESC-CMs can adhere, survive and form an sECM-based ECT with spontaneous contraction within 6 days of recellularization.

Accumulated data showed that long-term SDS treatment destroys the structure of ECM, and limits the following adhesion, survival and proliferation of seeding cells [28, 29]. Based on published literatures, we employed pretreatment/SDS/TritonX-100 three-step-method with shorter SDS treatment to obtain sECM. The whole decellularization procedure was much shorter than other reported procedure of sECM [16] and cECM [7]. Our results showed that the residual DNA contents of sECM in PreST group were less than 50 ng/mg, which is similar to the criteria proposed by Crapo and colleagues [30]. Meanwhile, the collagen fibers of sECM presented typical transverse periodic striations [31] with an average diameter far

less than 0.1 μm, which is similar to the diameter of cECM [4]. SECM in the present study showed a honeycomb-like endomysium structure and perimysium fibers, which is similar to the microstructure of cECM [7].

Ideal biocompatibility of scaffold for tissue engineering is one of the key factors to build a biomimetic engineered tissue. Generally, researchers hold the opinion that both cECM and sECM have high biological compatibility. CECM has been proven to be suitable for the adhesion, proliferation, differentiation and maturity of Sca-l$^+$ cardiac progenitor cells [4], neonatal CMs [4] and human MSCs [32]. Studies showed that dog sECM supports the adhesion, survival of human vascular peripheral stem cells, NIH3T3 fibroblasts and human microvascular endothelial cells for at least 7 days, and promotes the differentiation of C2C12 myoblasts [16]. In our study, sECM supported both mESCs and mESC-CMs for long-term survival and growth. Particularly, when mESCs were seeded on cECM and sECM under the same condition, more dead cells were observed on cECM. This result suggests that sECM possess well biological compatibility, and is more beneficial for the survival of differentiating mESCs.

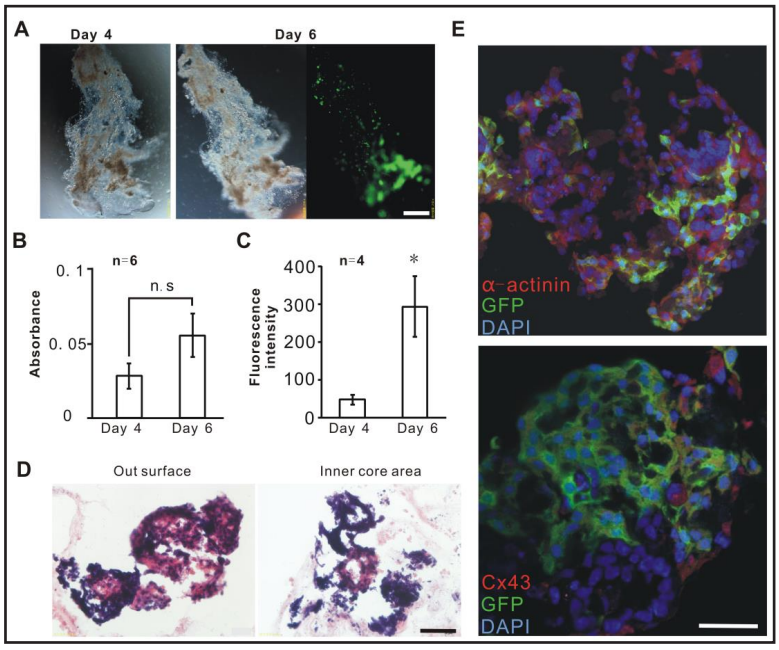

Fig. 4. SECM supports adhesion, survival and proliferation of mESC-CMs. (A) Representative light micrographs of sECM recellularized with purified mESC-CMs and fluorescence micrograph on day 6. GFP-positive cells were purified mESC-CMs. (B) LDH content detection showed the absorbance at day 4 and day 6 were extremely low and there were no difference between them. n = 6. (C) AlamarBlue assay showed fluorescence value at day 6 was significantly higher than it on day 4. n = 6; All data were presented as mean ± SEM in (B) and (C). *, p<0.05 vs. day 4. (D) Representative images of HE staining on day 7. (E) Representative images of immunofluorescent staining on day 7. Green: GFP; red: cardiac α-actinin (up) and Cx 43 (bottom); Blue: nuclei. Scale bar = 500 μm in (A), 20μm in (D) and 50 μm in (E).

Compared with cECM, sECM resulted in relatively higher NO secretion level when cocultured with mESCs, and lesser dead cells during recellularization. NO plays important regulatory roles in the cardiovascular systems. Both anti-apoptotic and pro-apoptotic functions of NO have been reported. NO inhibits myocardial apoptosis through a number of mechanisms independent of cGMP signaling pathway [33-35]. These mechanisms including prevention of caspase-3 activity via S-nitrosylation [33], activation of p38 MAPK [34], PI3-K/Akt [35] and reduction of mitochondrial Ca^{2+} uptake [36]. Therefore, greater NO secretion stimulated by sECM might account for better survival of seeding cells in our study.

Electrophysiology function is essential for the ECT. After transplantation, ideal ECT supposes to be paced by host heart. A recent study reported human iPS cell-derived CMs monolayer on biomatrix made of matrigel and PDMS are successively paced with different pacing frequencies from 0.7 Hz to 2.5 Hz [37]. In another report, the ECT composed with pig cECM and neonatal rat ventricular cells are response to different electrical stimulation from 1 to 5 Hz [10]. Consistently, our sECM-based cardiac tissue also shows electrical stimulated response under electrical stimulation from 0.5 Hz to 6 Hz. The β-adrenergic response is

another essential property of myocardium. Fong et al. seeded iPS cell-derived CMs into 3D cECM hydrogel to build ECT. They reported that ECT shows positive chronotropic response to β-adrenergic agonists Iso [38]. Another study also reported their ECT based on cECM and murine iPS cells shows an increased spontaneous frequency of FP in response to Iso [39]. We failed to record the spontaneous FP of ECT in our study, nevertheless, we observed the typical positive dromotropic response of sECM-based cardiac tissue derived from mESCs to Iso under electrical stimulation.

Table 7. Nitrite Concentration (μM) by mESC-CMs exposed to ECMs. N = 6 in each group. All data were presented as mean ± SEM. *, $p < 0.05$

	Sham	Native	PreST
cECM	2.99±0.65	5.42±0.86	2.91±0.68*
sECM	2.99±0.65	7.82±1.53	2.09±0.60*

Cx 43 plays a crucial role in forming myocardial gap junction, which maks cardiomyocytes a syncytial through electrical coupling [40]. Recently, Blazeski et al. found that neonatal CMs seeded on cECM could generate spontaneous contractions after incubation for 2 days. Cx 43 and α-actinin proteins were detected 7 days later [10]. Similarly, we recellularized sECM with the purified mESC-CMs and spontaneous synchronous rhythmic contraction also appeared after 4 days, with the detection of α-actinin and Cx 43 at day 6 of recellularization.

The limitation of the present study is lack of *in vivo* experiment. The effect of ECT patch on pathological heart has not been examined yet. Future work is still needed to further assess the fate of sECM-based ECT, and its effect on restoration of cardiac function by using animal model.

Conclusion

In summary, our findings demonstrated that sECMs had similar components and microstructure with cECM. SECMs had potential to replace cECMs to build a bioscaffold with low immunogenicity and good biocompatibility.

Acknowledgements

This study was supported by the National Natural Science Foundation of China (No. 31100828, 81401568 and 81472083), the Fundamental Research Funds for the Central Universities (HUST: 2017KFYXJJ058), the Fundamental Research Funds for the Undergraduates (HUST: 15A243), the National Undergraduate Training Programs for Innovation and Entrepreneurship (HUST: 201510487077).

Disclosure Statement

The authors declare that they have nothing to disclose.

References

1 D'Amore A, Yoshizumi T, Luketich SK, Wolf MT, Gu X, Cammarata M, Hoff R, Badylak SF, Wagner WR: Bi-layered polyurethane - Extracellular matrix cardiac patch improves ischemic ventricular wall remodeling in a rat model. Biomaterials 2016;107:1-14.

2 Jang J, Park HJ, Kim SW, Kim H, Park JY, Na SJ, Kim HJ, Park MN, Choi SH, Park SH, Kim SW, Kwon SM, Kim PJ, Cho DW: 3D printed complex tissue construct using stem cell-laden decellularized extracellular matrix bioinks for cardiac repair. Biomaterials 2017;112:264-274.

3 Ott HC, Matthiesen TS, Goh SK, Black LD, Kren SM, Netoff TI, Taylor DA: Perfusion-decellularized matrix: using nature's platform to engineer a bioartificial heart. Nat Med 2008;14:213-221.
4 Silva AC, Rodrigues SC, Caldeira J, Nunes AM, Sampaio-Pinto V, Resende TP, Oliveira MJ, Barbosa MA, Thorsteinsdottir S, Nascimento DS, Pinto-do OP: Three-dimensional scaffolds of fetal decellularized hearts exhibit enhanced potential to support cardiac cells in comparison to the adult. Biomaterials 2016;104:52-64.
5 Wainwright JM, Czajka CA, Patel UB, Freytes DO, Tobita K, Gilbert TW, Badylak SF: Preparation of cardiac extracellular matrix from an intact porcine heart. Tissue Eng Part C Methods 2010;16:525-532.
6 Jiang YD, Li WS, Yu C, Wang L, Sun XX, Xi JY: [Acquirement and evaluation of murine ventricular extracellular matrix]. Sheng li xue bao 2014;66:709-717.
7 Papalamprou A, Griffiths LG: Cardiac Extracellular Matrix Scaffold Generated Using Sarcomeric Disassembly and Antigen Removal. Ann Biomed Eng 2016;44:1047-1060.
8 French KM, Boopathy AV, DeQuach JA, Chingozha L, Lu H, Christman KL, Davis ME: A naturally derived cardiac extracellular matrix enhances cardiac progenitor cell behavior *in vitro*. Acta Biomater 2012;8:4357-4364.
9 Lu TY, Lin B, Kim J, Sullivan M, Tobita K, Salama G, Yang L: Repopulation of decellularized mouse heart with human induced pluripotent stem cell-derived cardiovascular progenitor cells. Nat Commun 2013;4:2307.
10 Blazeski A, Kostecki GM, Tung L: Engineered heart slices for electrophysiological and contractile studies. Biomaterials 2015;55:119-128.
11 Quarti A, Nardone S, Colaneri M, Santoro G, Pozzi M: Preliminary experience in the use of an extracellular matrix to repair congenital heart diseases. Interact Cardiovasc Thorac Surg 2011;13:569-572.
12 Tan MY, Zhi W, Wei RQ, Huang YC, Zhou KP, Tan B, Deng L, Luo JC, Li XQ, Xie HQ, Yang ZM: Repair of infarcted myocardium using mesenchymal stem cell seeded small intestinal submucosa in rabbits. Biomaterials 2009;30:3234-3240.
13 Potapova IA, Doronin SV, Kelly DJ, Rosen AB, Schuldt AJ, Lu Z, Kochupura PV, Robinson RB, Rosen MR, Brink PR, Gaudette GR, Cohen IS: Enhanced recovery of mechanical function in the canine heart by seeding an extracellular matrix patch with mesenchymal stem cells committed to a cardiac lineage. Am J Physiol Heart Circ Physiol 2008;295:H2257-2263.
14 Visone R, Gilardi M, Marsano A, Rasponi M, Bersini S, Moretti M: Cardiac Meets Skeletal: What's New in Microfluidic Models for Muscle Tissue Engineering. Molecules 2016;21
15 Gillies AR, Bushong EA, Deerinck TJ, Ellisman MH, Lieber RL: Three-dimensional reconstruction of skeletal muscle extracellular matrix ultrastructure. Microsc Microana 2014;20:1835-1840.
16 Wolf MT, Daly KA, Reing JE, Badylak SF: Biologic scaffold composed of skeletal muscle extracellular matrix. Biomaterials 2012;33:2916-2925.
17 Hanson KP, Jung JP, Tran QA, Hsu SP, Iida R, Ajeti V, Campagnola PJ, Eliceiri KW, Squirrell JM, Lyons GE, Ogle BM: Spatial and temporal analysis of extracellular matrix proteins in the developing murine heart: a blueprint for regeneration. Tissue Eng Part A 2013;19:1132-1143.
18 Eklund L, Piuhola J, Komulainen J, Sormunen R, Ongvarrasopone C, Fassler R, Muona A, Ilves M, Ruskoaho H, Takala TE, Pihlajaniemi T: Lack of type XV collagen causes a skeletal myopathy and cardiovascular defects in mice. Proc Natl Acad Sci U S A 2001;98:1194-1199.
19 Osses N, Brandan E: ECM is required for skeletal muscle differentiation independently of muscle regulatory factor expression. Am J Physiol Cell Physiol 2002;282:C383-394.
20 Merritt EK, Cannon MV, Hammers DW, Le LN, Gokhale R, Sarathy A, Song TJ, Tierney MT, Suggs LJ, Walters TJ, Farrar RP: Repair of traumatic skeletal muscle injury with bone-marrow-derived mesenchymal stem cells seeded on extracellular matrix. Tissue Eng Part A 2010;16:2871-2881.
21 Porzionato A, Sfriso MM, Pontini A, Macchi V, Petrelli L, Pavan PG, Natali AN, Bassetto F, Vindigni V, De Caro R: Decellularized Human Skeletal Muscle as Biologic Scaffold for Reconstructive Surgery. Int J Mol Sci 2015;16:14808-14831.
22 DeQuach JA, Lin JE, Cam C, Hu D, Salvatore MA, Sheikh F, Christman KL: Injectable skeletal muscle matrix hydrogel promotes neovascularization and muscle cell infiltration in a hindlimb ischemia model. Eur Cells Mater 2012;23:400-412; discussion 412.
23 Xi J, Khalil M, Spitkovsky D, Hannes T, Pfannkuche K, Bloch W, Saric T, Brockmeier K, Hescheler J, Pillekamp F: Fibroblasts support functional integration of purified embryonic stem cell-derived cardiomyocytes into avital myocardial tissue. Stem Cells Dev 2011;20:821-830.

24 Luo X, Zhong B, Hong X, Cui Y, Gao Y, Yin M, Tang M, Hescheler J, Xi J: Puerarin Exerts a Delayed Inhibitory Effect on the Proliferation of Cardiomyocytes Derived from Murine ES Cells via Slowing Progression through G2/M Phase. Cell Physiol Biochem 2016;38:1333-1342.
25 Kolossov E, Bostani T, Roell W, Breitbach M, Pillekamp F, Nygren JM, Sasse P, Rubenchik O, Fries JW, Wenzel D, Geisen C, Xia Y, Lu Z, Duan Y, Kettenhofen R, Jovinge S, Bloch W, Bohlen H, Welz A, Hescheler J, Jacobsen SE, Fleischmann BK: Engraftment of engineered ES cell-derived cardiomyocytes but not BM cells restores contractile function to the infarcted myocardium. J Exp Med 2006;203:2315-2327.
26 Livak KJ, Schmittgen TD: Analysis of relative gene expression data using real-time quantitative PCR and the 2(-Delta Delta C(T)) Method. Methods 2001;25:402-408.
27 Lai YJ, Huang EY, Yeh HI, Chen YL, Lin JJ, Lin CI: On the mechanisms of arrhythmias in the myocardium of mXinalpha-deficient murine left atrial-pulmonary veins. Life Sci 2008;83:272-283.
28 Gui L, Chan SA, Breuer CK, Niklason LE: Novel utilization of serum in tissue decellularization. Tissue Eng Part C Methods 2010;16:173-184.
29 Momtahan N, Panahi T, Poornejad N, Stewart MG, Vance BR, Struk JA, Castleton AA, Roeder BL, Sukavaneshvar S, Cook AD: Using Hemolysis as a Novel Method for Assessment of Cytotoxicity and Blood Compatibility of Decellularized Heart Tissues. ASAIO J 2016;62:340-348.
30 Crapo PM, Gilbert TW, Badylak SF: An overview of tissue and whole organ decellularization processes. Biomaterials 2011;32:3233-3243.
31 Ushiki T: Collagen fibers, reticular fibers and elastic fibers. A comprehensive understanding from a morphological viewpoint. Arch Histol Cytol 2002;65:109-126.
32 Kc P, Shah M, Liao J, Zhang G: Prevascularization of Decellularized Porcine Myocardial Slice for Cardiac Tissue Engineering. ACS Appl Mater Interfaces 2017;9:2196-2204.
33 Maejima Y, Adachi S, Morikawa K, Ito H, Isobe M: Nitric oxide inhibits myocardial apoptosis by preventing caspase-3 activity via S-nitrosylation. J Mol Cell Cardiol 2005;38:163-174.
34 Rakhit RD, Kabir AN, Mockridge JW, Saurin A, Marber MS: Role of G proteins and modulation of p38 MAPK activation in the protection by nitric oxide against ischemia-reoxygenation injury. Biochem Biophys Res Commun 2001;286:995-1002.
35 Mockridge JW, Marber MS, Heads RJ: Activation of Akt during simulated ischemia/reperfusion in cardiac myocytes. Biochem Biophys Res Commun 2000;270:947-952.
36 Rakhit RD, Mojet MH, Marber MS, Duchen MR: Mitochondria as targets for nitric oxide-induced protection during simulated ischemia and reoxygenation in isolated neonatal cardiomyocytes. Circulation 2001;103:2617-2623.
37 Herron TJ, Rocha AM, Campbell KF, Ponce-Balbuena D, Willis BC, Guerrero-Serna G, Liu Q, Klos M, Musa H, Zarzoso M, Bizy A, Furness J, Anumonwo J, Mironov S, Jalife J: Extracellular Matrix-Mediated Maturation of Human Pluripotent Stem Cell-Derived Cardiac Monolayer Structure and Electrophysiological Function. Circ Arrhythm Electrophysiol 2016;9:e003638.
38 Fong AH, Romero-López M, Heylman CM, Keating M, Tran D, Sobrino A, Tran AQ, Pham HH, Fimbres C, Gershon PD, Botvinick EL, George SC, Hughes CC: Three-dimensional adult cardiac extracellular matrix promotes maturation of human induced pluripotent stem cell-derived cardiomyocytes. Tissue Eng Part A 2016.
39 Kensah G, Roa Lara A, Dahlmann J, Zweigerdt R, Schwanke K, Hegermann J, Skvorc D, Gawol A, Azizian A, Wagner S, Maier LS, Krause A, Drager G, Ochs M, Haverich A, Gruh I, Martin U: Murine and human pluripotent stem cell-derived cardiac bodies form contractile myocardial tissue *in vitro*. Eur Heart J 2013;34:1134-1146.
40 Schulz R, Gorge PM, Gorbe A, Ferdinandy P, Lampe PD, Leybaert L: Connexin 43 is an emerging therapeutic target in ischemia/reperfusion injury, cardioprotection and neuroprotection. Pharmacol Ther 2015;153:90-106.